Nuclear Instruments and Methods in Physics Research A 391 (1997) 42–51

ELSEVIER

NUCLEAR INSTRUMENTS & METHODS IN PHYSICS RESEARCH Section A

Simulation of electron cooling and intrabeam scattering processes of a heavy ion beam in HIRFL-CSR

Y.N. Rao[a,*], T. Katayama[b]

[a]*Institute of Modern Physics, Chinese Academy of Sciences, P.O. Box 31, 730000, Lanzhou, PR China*
[b]*Institute for Nuclear Study, University of Tokyo, Tanashi, Tokyo 188, Japan*

Abstract

This paper is devoted to the simulation of electron cooling and intrabeam scattering processes of a heavy ion beam in the proposed HIRFL-CSR, according to the analytical cooling force formulae and the intrabeam scattering growth rate expressions. Some important effects like the betatron and synchrotron oscillations, and space charge effect of the electron beam have been considered. Time evolution of beam emittances and momentum spread under joint action of the electron cooling and intrabeam scattering are shown. The dependence of ion beam properties in equilibrium on the number of particles and the electron current are presented.

PACS: 29.27a
Keywords: Electron cooling; Intra-beam scattering; Equilibrium emittance

1. Introduction

The phase space density of the cooled ion beam in a storage ring is raised through electron cooling. However, the ion beam cannot be cooled to infinitely small emittances and momentum spread because of heating. In the static operation of a heavy ion storage ring with electron cooling at constant energy, intrabeam scattering is the dominant heating mechanism [1] which determines the resolution limits of the cooled ion beam.

This paper aims at simulation of the electron cooling and the intrabeam scattering (IBS) processes for a bunched heavy ion beam of Ar^{18+} of 25 MeV/u in the proposed HIRFL-CSR [2] by using the analytical cooling force formulae of Meshkov [3] and the extended Piwinski intrabeam scattering growth rate expressions [4]. Some peculiarities, such as betatron and synchrotron oscillations of a particle, the electron beam space charge effect and dispersion in the cooling section, are taken into account [5]. The variations of beam emittances and momentum spread obtained from the simulations are shown as a function of time. After that, the dependence of ion beam emittances and momentum spread in equilibrium between the electron cooling and intrabeam scattering on the number of particles as well as the cooling electron current are described.

2. Description of the simulation processes

2.1. Electron cooling

The calculation of the electron cooling process is based upon the cooling force. However, the complicated dependence of the cooling force on parameters makes it difficult to calculate the cooling process analytically. Taking into account the betatron and synchrotron oscillations (in the presence of RF voltage) of a single particle and the space charge effect of the electron beam, the electron cooling process is simulated [5].

* Corresponding author. Fax: +86 931 888 1100, e-mail: raoyn@csraxp.lzb.ac.cn

PII S0168-9002(97)00023-5

2.1.1. Betatron and synchrotron oscillations

In the simulation procedure, the ring is divided into two parts, the first part from the cooling section exit (labeled with subscript 0) up to its entrance (labeled with subscript 1), and the second part going through the cooling section. After one turn in the ring, the phase of the inspected ion with respect to the RF and its relative momentum spread are described by phase motion equations [6]:

$$\frac{\mathrm{d}\phi}{\mathrm{d}t} = h\omega_s\eta_p\frac{\Delta P}{P_s}, \tag{1}$$

$$\frac{\mathrm{d}}{\mathrm{d}t}\left(\frac{\Delta P}{P_s}\right) = \frac{\omega_s}{2\pi}\frac{qeU_a}{AM_nc^2\beta^2\gamma}(\cos\phi - \cos\phi_s), \tag{2}$$

where h is the RF harmonic number, ω_s is the revolution angular frequency of the synchronous ion, $\eta_p = |1/\gamma^2 - 1/\gamma_{tr}^2|$, γ_{tr} is the transition energy factor of the ring, U_a is the amplitude of the RF voltage, $M_nc^2 = 931.501\ \mathrm{MeV}/u$ is the rest energy per nucleon, and c is the speed of light.

From the above equations, one gets the phase and momentum spread of the ion at the entrance of the cooling section:

$$\phi_1 = \phi_0 + h2\pi(1-\eta_{ec})\eta_p\left(\frac{\Delta P}{P_s}\right)_0, \tag{3}$$

$$\left(\frac{\Delta P}{P_s}\right)_1 = \left(\frac{\Delta P}{P_s}\right)_0 + \frac{qeU_a}{AM_nc^2\beta^2\gamma}(1-\eta_{ec})(\cos\phi_1 - \cos\phi_s). \tag{4}$$

The horizontal and vertical (designated by subscript h and v respectively) betatron positions and divergences after passage through the first part are given by the following matrix expression [7]:

$$\begin{pmatrix} x_j \\ \theta_j \end{pmatrix}_1 = \begin{bmatrix} \cos(\mu_j) + \alpha_j\sin(\mu_j) & \beta_j\sin(\mu_j) \\ -\gamma_j\sin(\mu_j) & \cos(\mu_j) - \alpha_j\sin(\mu_j) \end{bmatrix} \cdot \begin{pmatrix} x_j \\ \theta_j \end{pmatrix}_0, \quad j = \mathrm{h}, \mathrm{v}, \tag{5}$$

in which $\mu_j = 2\pi\nu_j(1-\eta_{ec})$, $\nu_j = Q_j + \xi_j\cdot\Delta P/P_s$, μ_j is the betatron phase shift of the inspected ion after the first part, ν_j and Q_j are the betatron wave numbers of the inspected ion and the synchronous ion respectively, $\eta_{ec} = L_{cooler}/C$ is the fraction of the cooling section length to the ring perimeter, ξ_j is the chromaticity of the machine, and α_j, β_j and γ_j are the Twiss parameters at the entrance or exit of the cooling section (symmetric points).

Without loss of generality, one assumes that the ion is initially located at point I of the transverse phase ellipse shown in Fig. 1; the betatron position and divergence correspond to

$$\begin{pmatrix} x_j \\ \theta_j \end{pmatrix}_0 = \begin{pmatrix} 0 \\ \sqrt{\varepsilon_{j0}/(\pi\beta_j)} \end{pmatrix}. \tag{6}$$

On each passage through the cooling section, the ion experiences a cooling force which decreases the velocity

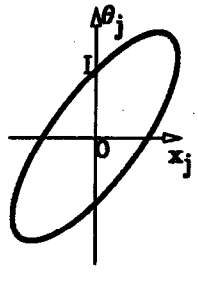

Fig. 1. Transverse betatron ellipse of ion beam.

components but does not change the position coordinates much. In the lab frame, the cooling differential equations are expressed as

$$\frac{\mathrm{d}\theta_j}{\mathrm{d}s} = \frac{F_j}{AM_\mathrm{n}c^2\beta^2\gamma}, \tag{7}$$

$$\frac{\mathrm{d}}{\mathrm{d}s}\left(\frac{\Delta P}{P_\mathrm{s}}\right) = \frac{F_\mathrm{l}}{AM_\mathrm{n}c^2\beta^2\gamma} \tag{8}$$

in which $0 \le s \le L_{\mathrm{cooler}}$, and F_j and F_l denote transverse and longitudinal cooling forces respectively.

Through numerical integration of Eqs. (7) and (8), one can obtain θ_j and $\Delta P/P_\mathrm{s}$ values at the exit of cooling section. In the practical evaluations, the difference method is used to solve the above equations, that is

$$\delta\theta_j = \frac{F_j}{AM_\mathrm{n}c^2\beta^2\gamma}\delta s, \qquad \delta\left(\frac{\Delta P}{P_\mathrm{s}}\right) = \frac{F_\mathrm{l}}{AM_\mathrm{n}c^2\beta^2\gamma}\delta s,$$

where δs is chosen such that [5] $|\delta\theta_j| \le 0.05|\theta_j|$ and $|\delta(\Delta P/P_\mathrm{s})| \le 0.05|\Delta P/P_\mathrm{s}|$. Following these criteria, the cooling section is divided successively into two equal segments. After each sub-segment, the divergences and momentum spread are changed as $\theta_j + \delta\theta_j$ and $\Delta P/P_\mathrm{s} + \delta(\Delta P/P_\mathrm{s})$ which are taken as starting values for the next segment, up to the whole cooling section traversal.

After traversal of the cooling section, the phase angle and betatron positions of the ion are approximately unchanged, i.e.

$$\phi_1 \simeq \phi_0, \qquad (x_j)_1 \simeq (x_j)_0.$$

2.1.2. Cooling force

As mentioned above, the behavior of the ion after transmission through the cooling section depends on the cooling force.

The formulae of the cooling force in the lab frame may be expressed as [3,5]

$$\boldsymbol{F}_j^{\mathrm{lf}} = -2\pi\frac{I_\mathrm{e}}{\pi r_\mathrm{b}^2 e\beta\gamma c}Q_\mathrm{i}^2 r_\mathrm{e}^2 m_\mathrm{e}c^2\frac{\boldsymbol{\theta}_j}{\beta^2\gamma^2}\begin{cases}\dfrac{1}{\theta^3}(2L_{\mathrm{FH}} + K_\mathrm{t}L_{\mathrm{MH}}), & \theta > \theta_{\mathrm{et}},\\ \dfrac{2}{\theta_{\mathrm{et}}^3}(L_{\mathrm{FL}} + N_\mathrm{L}L_{\mathrm{AL}}) + K_\mathrm{t}\dfrac{L_{\mathrm{ML}}}{\theta^3}, & \theta_{\mathrm{el}} < \theta < \theta_{\mathrm{et}},\\ \dfrac{2}{\theta_{\mathrm{et}}^3}(L_{\mathrm{FS}} + N_\mathrm{S}L_{\mathrm{AS}}) + \dfrac{L_{\mathrm{MS}}}{\theta_{\mathrm{el}}^3}, & \theta < \theta_{\mathrm{el}},\end{cases}$$

$$\boldsymbol{F}_l^{\mathrm{lf}} = -2\pi\frac{I_\mathrm{e}}{\pi r_\mathrm{b}^2 e\beta\gamma c}Q_\mathrm{i}^2 r_\mathrm{e}^2 m_\mathrm{e}c^2\frac{\boldsymbol{\theta}_l}{\beta^2\gamma^2}\begin{cases}\dfrac{1}{\theta^3}(2L_{\mathrm{FH}} + K_\mathrm{l}L_{\mathrm{MH}} + 2), & \theta > \theta_{\mathrm{et}},\\ \dfrac{2}{\theta_{\mathrm{et}}^2\theta_\mathrm{l}}(L_{\mathrm{FL}} + N_\mathrm{L}L_{\mathrm{AL}}) + (K_\mathrm{l}L_{\mathrm{ML}} + 2)\dfrac{1}{\theta^3}, & \theta_{\mathrm{el}} < \theta < \theta_{\mathrm{et}},\\ \dfrac{2}{\theta_{\mathrm{et}}^2\theta_{\mathrm{el}}}(L_{\mathrm{FS}} + N_\mathrm{S}L_{\mathrm{AS}}) + \dfrac{L_{\mathrm{MS}}}{\theta_{\mathrm{el}}^3}, & \theta < \theta_{\mathrm{el}},\end{cases}$$

in which

$$K_\mathrm{t} = 1 - 3\left(\frac{\theta_\mathrm{l}}{\theta}\right)^2, \qquad K_\mathrm{l} = 3 - 3\left(\frac{\theta_\mathrm{l}}{\theta}\right)^2$$

and the Coulomb logarithms are given as follows:

$$L_{FH}=\ln\left(\frac{\beta^3\gamma^3 c\theta^3}{Q_i\omega_e r_e}\right),\quad L_{MH}=\max\left[\ln\left(\frac{\omega_c}{\omega_{pe}}\frac{\theta}{\theta_{et}}\right),\quad \ln\left(\frac{\omega_c}{\beta\gamma c\theta_{et}}\left(\frac{3Q_i}{n_e}\right)^{1/3}\right)\right],$$

$$L_{FL}=\ln\left(\frac{\beta^3\gamma^3\theta_{et}^2\theta c}{Q_i\omega_e r_e}\right),\ L_{AL}=\ln\left(\frac{\theta_{et}}{\theta}\right),$$

$$L_{ML}=L_{MH},\qquad L_{FS}=\ln\left(\frac{\beta^3\gamma^3 c\theta_{et}^2\theta_{el}}{Q_i\omega_c r_e}\right),$$

$$L_{AS}=\ln\left(\frac{\theta_{et}}{\theta_{el}}\right),\qquad L_{MS}=\max\left[\ln\left(\frac{\omega_e}{\omega_{pe}}\frac{\theta_{el}}{\theta_{et}}\right),\quad \ln\left(\frac{\omega_c}{\beta\gamma c\theta_{et}}\left(\frac{3Q_i}{n_e}\right)^{1/3}\right)\right],$$

$$N_L=\left[\frac{\theta_{et}}{\pi\theta}\right],\qquad N_S=\left[\frac{\theta_{et}}{\pi\theta_{el}}\right],$$

where $\omega_e=eB_0/m_e$ is the electron cyclotron frequency in the longitudinal magnetic field B_0, $\omega_{pe}=\sqrt{n_e 4\pi r_e}c$ is the frequency of electron plasma, and n_e is the electron density.

2.1.3. Electron beam space charge

Because of the electron beam space charge depression, electrons at different radii inside the beam have different longitudinal velocities. Accordingly, the longitudinal velocity component of an ion at a certain radius should be defined with respect to that of an electron at the same radius.

Following the electrostatic Gaussian theorem, one finds the radial electric field at radius r:

$$\boldsymbol{E}=-\frac{I_e}{2\pi\varepsilon_0 r_b^2\beta c}\boldsymbol{r},\qquad 0\le r\le r_b,$$

which results in a potential difference

$$\Delta U=-\int_0^r \boldsymbol{E}\cdot d\boldsymbol{r}=\frac{I_e}{4\pi\varepsilon_0\beta c}\frac{r^2}{r_b^2}$$

in which ε_0 is the permittivity of free space. Therefore, the relative momentum deviation of an electron at radius r from that on axis is given by

$$\frac{\Delta P_e}{P_s}=\frac{\gamma}{\gamma+1}\frac{\Delta W_e}{W_s}=\frac{I_e}{4\pi\varepsilon_0\beta^3 c}\frac{e}{m_e c^2\gamma}\frac{r^2}{r_b^2}. \tag{9}$$

Signifying by f_n the neutralization factor of the space charge, one gets the divergence deviation θ_l^n given by

$$\theta_l^n=\theta_l-\frac{1}{\gamma}\frac{\Delta P_e}{P_s}$$

$$=\theta_l-\frac{I_e}{4\pi\varepsilon_0\beta^3 c}\frac{e}{m_e c^2\gamma^2}\frac{r^2}{r_b^2}(1-f_n)$$

in which the radius r is related to the horizontal dispersion D_h in the cooling section by

$$r=\sqrt{\left(D_h\frac{\Delta P}{P_s}+x_h\right)^2+x_v^2}.$$

θ_l is replaced by θ_l^n in the above cooling force formulae for practical calculations. When the condition $r>r_b$ is met on a certain passage through the cooling section, the cooling force is set to zero since the ion is outside the electron beam.

The momentum spread $\Delta P/P_s$ of the ion and its coordinates in transverse phase space (x_j, θ_j) are recorded at the exit of the cooling section on each turn. The point (x_j, θ_j) is positioned on an ellipse, and the elliptic equation is connected with the local Twiss parameters by

$$\gamma_j x_j^2 + 2\alpha_j x_j \theta_j + \beta_j \theta_j^2 = \varepsilon_j ,$$

where ε_j is the Courant–Snyder invariant [7], and $\pi\varepsilon_j$ stands for the beam emittance.

2.1.4. Simulation results in CSR

A computer program has been made to simulate the cooling process of the ion beam in the storage ring on the basis of the above principle. An application is dedicated to the cooling of the typical ion beam $^{40}Ar^{18+}$ at injection into CSR. Typical parameters involved in the calculations are listed in Table 1. Actually, both the electron beam transverse temperature and the neutralization factor of the electron beam space charge have a significant influence on the cooling rate [8], values of kT_t and f_n are taken to be 0.02 eV and 90%, respectively, in these calculation. In addition, the initial ε_h value is 125π mm mrad, much larger than ε_v, due to the multiturn injection horizontally. In the simulation, the horizontal and vertical betatron oscillations are assumed to be fully uncoupled by some means.

Fig. 2 shows the resultant reduction of ε_h, ε_v and $\Delta P/P_s$ with time. $\Delta P/P_s$ of the inspected ion is decreased in oscillation, and the oscillation amplitude corresponds to momentum spread of the beam.

2.2. Intrabeam scattering

The intrabeam scattering growth rates are connected with the 6-dimensional phase space density of the ion beam and the specific ion optics of the storage ring. Usually, the growth rates are described by the relative time derivatives of rms betatron angles σ_h', σ_v', and rms relative momentum spread σ_p.

It is frequently assumed that the betatron amplitude would grow at the same rate as the betatron angle, and,

Table 1
Parameters used in the simulation

Storage ring parameters	
Ring perimeter C [m]	141.05
Length of cooling section L_{cooler} [m]	3.0
Betatron tune	$Q_h = 3.4516$, $Q_v = 2.8893$
β value in cooling section [m]	$\beta_h = 8.0$, $\beta_v = 15.0$
α value in cooling section	$\alpha_h = 0.0$, $\alpha_v = 0.0$
Dispersion in cooling section D_h [m]	0.0
Transition gamma γ_{tr}	4.359
Chromaticity	$\xi_h = -4.907$, $\xi_v = -3.988$
RF harmonic number h	7
RF voltage amplitude U_a [V]	4000
Period of synchrotron oscillation [μs]	343.33
Electron beam parameters	
Electron energy [keV]	13.71
Average velocity β [c]	0.227
Electron beam radius r_b [mm]	32
Electron beam current I_e [A]	2.0
Electron density n_e [cm^{-3}]	5.7×10^7
Neutralization factor f_n	90%
Transverse temperature kT_t [eV]	0.02
Longitudinal temperature kT_l [eV]	5.0×10^{-4}
Transverse rms velocity Δ_t [m/s]	5.93×10^4
Longitudinal rms velocity Δ_l [m/s]	9.38×10^3
Solenoid field strength B_0 [G]	1000
Ion beam parameters before cooling	
Ion	$^{40}Ar^{18+}$
Energy [MeV/u]	25
Transverse emittances [πmm mrad]	$\varepsilon_{h0} = 125$, $\varepsilon_{v0} = 10$
Momentum spread $(\Delta P/P_s)_0$	$\pm 1.5 \times 10^{-3}$

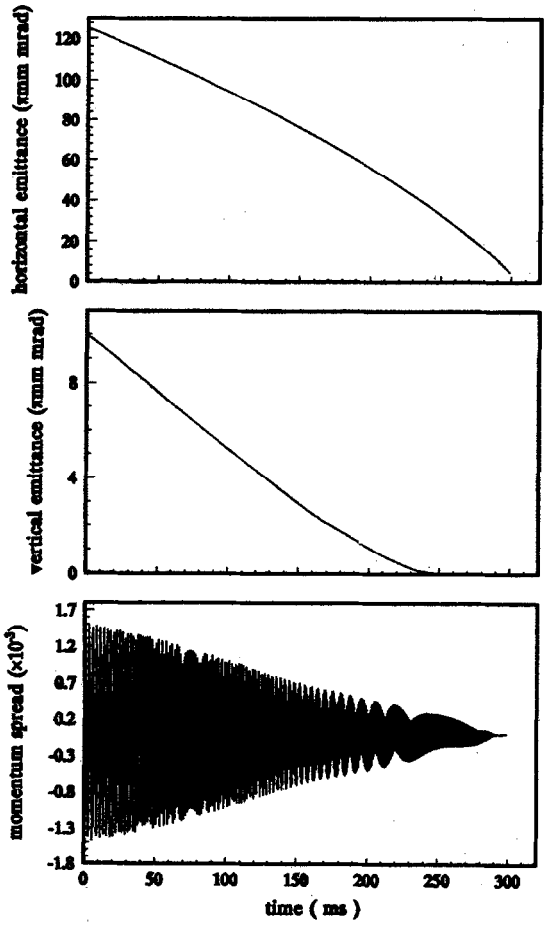

Fig. 2. Decrease of the horizontal and vertical emittances and the momentum spread with electron cooling for an Ar^{18+} beam of 25 MeV/u.

for a bunched beam, the bunch length would grow at the same rate as the momentum spread. As a consequence, there is a factor of 2 between the emittance growth rates and the angle growth rates:

$$\frac{1}{\varepsilon_l}\frac{\mathrm{d}\varepsilon_l}{\mathrm{d}t} = 2\frac{1}{\sigma_p}\frac{\mathrm{d}\sigma_p}{\mathrm{d}t}, \qquad \frac{1}{\varepsilon_j}\frac{\mathrm{d}\varepsilon_j}{\mathrm{d}t} = 2\frac{1}{\sigma'_j}\frac{\mathrm{d}\sigma'_j}{\mathrm{d}t}.$$

The extended Piwinski IBS growth rate formulae are used to investigate the beam blow-up. These formulae are given in Eq. (33) of Ref. [4]. Starting from the exit of the cooling section with given initial emittances ε_{j0}, the three emittance growth times (inverse of the growth rates) are calculated at a series of lattice points through numerical integration to the scattering functions [4], and then averaged around the ring. The three emittances grow to be

$$\varepsilon_j = \varepsilon_{j0}\, \mathrm{e}^{t/\tau_j}$$

after N_{ibs} turns. N_{ibs} is given by

$$N_{\mathrm{ibs}} = \mathrm{frac}\,\frac{\min(\tau_h, \tau_v, \tau_l)}{\tau_c}$$

in which τ_j ($j = \mathrm{h}, \mathrm{v}, \mathrm{l}$) are the e^{-1} emittance growth times in three degrees of freedom, τ_c is the revolution period of the ion and frac is a factor (for example 0.1) for adjustment of the N_{ibs} value.

Due to the growth of emittances, the coordinates on the phase ellipses of the ion at the entrance of the cooling section after N_{ibs} turns are increased by a factor

$$\sqrt{\frac{\varepsilon_j}{\varepsilon_{j0}}} = \mathrm{e}^{t/2\tau_j}$$

in which a small amplitude approximation [9] is employed for the synchrotron oscillation, and the ion is assumed to be still positioned on an ellipse after scattering.

Fig. 3 exemplifies the calculated IBS blow-up of a 25 MeV/u $^{40}Ar^{18+}$ beam of 5.0×10^8 particles/bunch after electron cooling, supposing horizontal and vertical emittances of 1.0π mm mrad and a momentum spread of $\pm 1.0 \times 10^{-4}$ initially.

2.3. Equilibrium between electron cooling and IBS

In principle, the time evolution of the beam behaviour under joint actions of the electron cooling and intrabeam scattering may be described by the differential equations

$$\frac{\mathrm{d}\varepsilon}{\mathrm{d}t} = \frac{\mathrm{d}\varepsilon_{\mathrm{ec}}}{\mathrm{d}t} + \frac{\mathrm{d}\varepsilon_{\mathrm{ibs}}}{\mathrm{d}t}, \qquad \frac{\mathrm{d}\left(\frac{\Delta P}{P}\right)}{\mathrm{d}t} = \frac{\mathrm{d}\left(\frac{\Delta P}{P}\right)_{\mathrm{ec}}}{\mathrm{d}t} + \frac{\mathrm{d}\left(\frac{\Delta P}{P}\right)_{\mathrm{ibs}}}{\mathrm{d}t}.$$

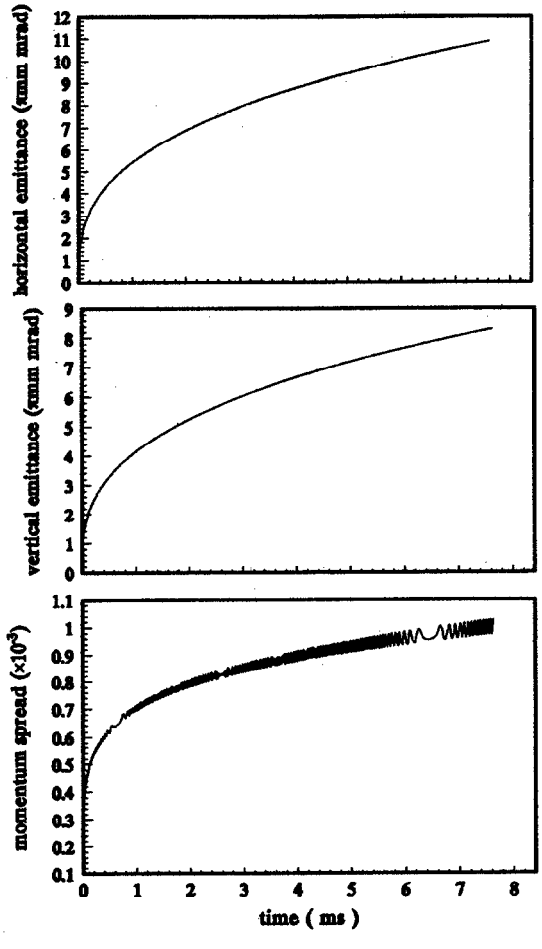

Fig. 3. Blow-up of the horizontal and vertical emittances, and the momentum spread with IBS for an Ar^{18+} beam of 25 MeV/u.

The equilibrium properties are obtained from the conditions

$$\frac{d\varepsilon}{dt} = 0, \qquad \frac{d\left(\frac{\Delta P}{P}\right)}{dt} = 0$$

In the practical equilibrium simulations, both the electron cooling and the IBS are calculated according to the procedures described above. With the proceeding of the cooling process, the IBS growth times τ_j become shorter and shorter, even $\tau_j < \tau_c$ is taking place. In this case, beam blow-up due to the IBS should be evaluated one location by one location from the exit up to the entrance of the ring. When the rms value of the relative changes of emittances during some time interval is smaller than a given tolerance, i.e. the condition

$$\sqrt{\left(\frac{d\varepsilon_h}{\varepsilon_h}\right)^2 + \left(\frac{d\varepsilon_v}{\varepsilon_v}\right)^2 + \left(\frac{d\varepsilon_l}{\varepsilon_l}\right)^2} \leq \text{tole.}$$

is fulfilled, an equilibrium is arrived at.

Fig. 4 shows variations of transverse emittances and momentum spread with time under the combined actions of the IBS and electron cooling with electron current $I_e = 2.0$ A and particle numbers $N_i = 5.0 \times 10^8$ per bunch. The initial value of the horizontal and vertical emittances (2σ) and the momentum spread (2σ) are 125π mm mrad, 10π mm · mrad and $\pm 1.5 \times 10^{-3}$ respectively. The results demonstrate that the IBS comes into

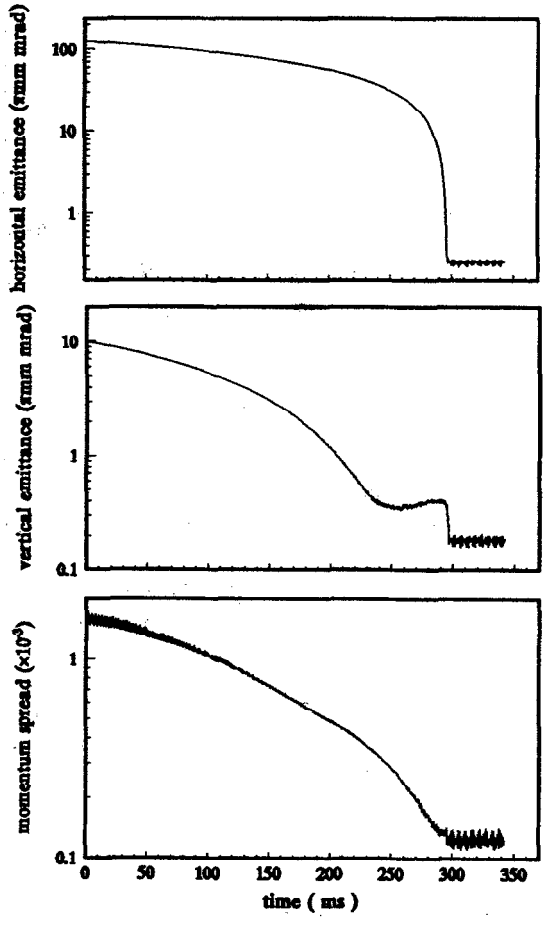

Fig. 4. The time evolution of beam emittances and momentum spread with electron cooling and IBS.

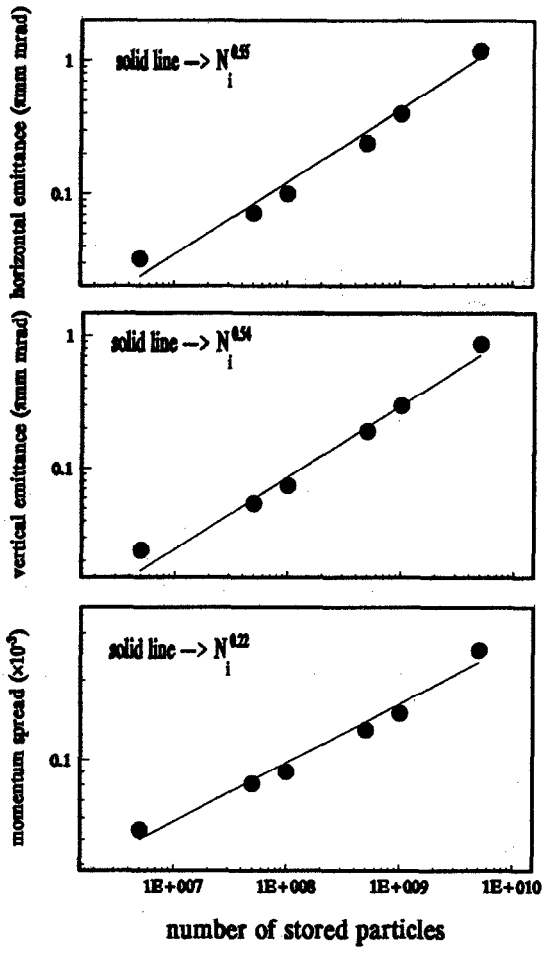

Fig. 5. Equilibrium emittances and momentum spread as a function of number of stored ions for $I_e = 2.0$ A.

the function significantly when the emittances and momentum spread are cooled down to values lower than $\sim 0.5\pi$ mm mrad and $\sim 0.5 \times 10^{-3}$ respectively.

Simulation results of the emittance and momentum spread as a function of the number of stored particles for an Ar^{18+} beam cooled with $I_e = 2.0$ A are shown in Fig. 5. An increase of the phase space volume with the number of stored ions N_i is evident. The momentum spread shows a $N_i^{0.22}$-dependence, whereas horizontal and vertical emittances grow with $N_i^{0.55}$.

The equilibrium state must depend on the electron beam current which determines the cooling rate. A higher electron intensity results in an increased cooling rate which corresponds to a lower equilibrium temperature of the ion beam. Assuming an independence of the electron beam transverse temperature kT_e on the electron current up to 2.0 A, i.e. the remaining kT_e is constant at 0.02 eV, the calculated ion beam emittances and momentum spread as a function of the electron current are shown in Fig. 6.

The momentum spread dependence is close to $I_e^{-0.31}$; the decrease of the horizontal and vertical emittances can be described by $I_e^{-0.65}$ and $I_e^{-0.59}$ respectively.

3. Summary and discussion

We demonstrate the simulation results of the equilibrium property of the cooled ion beam, assuming a balance between the electron cooling and intrabeam scattering. Although the equilibrium properties are related to

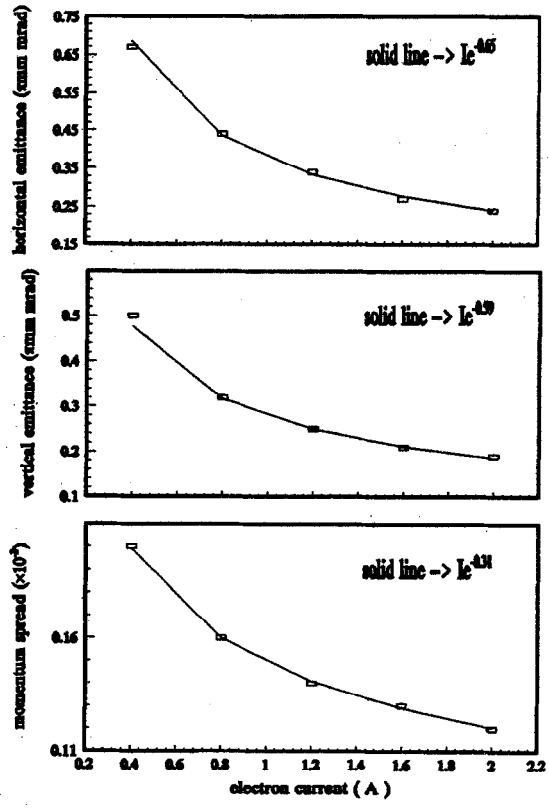

Fig. 6. Equilibrium emittances and momentum spread as a function of electron current for $N_i = 5.0 \times 10^8$/bunch.

practical cooling conditions, the simulation results show scaling rules which are quantitatively the same as the measurements at ESR.

Strictly speaking, a nonlinear force may deform the phase ellipse of an ion beam, and make particles which are on the same elliptic curve initially have a different locus in phase space. However, results from the simulation of 300 particles (200 of them located on an identical ellipse in the beginning) demonstrate that the phase space deformation due to the nonlinear electron cooling forces is quite small, and the maximum relative difference of the elliptic areas of the 200 particles is less than 2%. Therefore a single particle is used in the above simulation.

References

[1] M. Steck et al., Workshop on Beam Cooling and Related Topics, Montreux, 4–8 Oct. 1993, CERN 94-03 (1993) p. 395; M. Steck et al., Proc. 3rd Europ. Particle Accelerator Conf., Berlin, 1992), p. 827.
[2] J.W. Xia and B.W. Wei, The HIRFL-CSR Proposal, Proc. 15th Int. Conf. on Cyclotrons and their Applications, 1995.
[3] I.N. Meshkov, Phys. Part. Nucl. 25 (1994) 631.
[4] M. Martini, CERN PS/84-9(AA) (1984); R. Giannini and D. Mohl, CERN PS/AR/Note 92-22 (1993).
[5] A. Yu Lavrentev and I.N. Meshkov, JINR, Dubna, E9-95-317 (1995).
[6] J. Le Duff, CERN 94-01 (1994) p. 289.
[7] E.D. Courant and H.S. Snyder, Annals of Physics 3 (1958) 1.
[8] Y.N. Rao et al., Simulation of electron cooling process in a storage ring, High Energy Phys. Nucl. Phys., to be published.
[9] M. Conte and W. Mackay, Physics of Particle Accelerators (World Scientific, 1991).